catalysts

MDPI

Article

Rational Engineering of *Mesorhizobium* Imine Reductase for Improved Synthesis of *N*-Benzyl Cyclo-tertiary Amines

Zi-Han Zhang, An-Qi Wang, Bao-Di Ma and Yi Xu *

School of Chemical and Environmental Engineering, Shanghai Institute of Technology, Shanghai 201418, China; 206061251@mail.sit.edu.cn (Z.-H.Z.); 226061271@mail.sit.edu.cn (A.-Q.W.); mbd2966@sit.edu.cn (B.-D.M.)
* Correspondence: xuyi@sit.edu.cn; Tel.: +86-21-60873024

Abstract: The effective synthesis of *N*-benzyl cyclo-tertiary amines using imine reductase, key components in natural products and pharmaceutical synthesis, is a green approach. Traditional methods faced challenges with enzyme activity and selectivity. This study focused on enhancing *Mesorhizobium* imine reductase (*Mes*IRED) for better *N*-benzyl cyclo-tertiary amine production. Through alanine scanning and consensus mutation, 12 single-site *Mes*IRED mutants were identified from 23 candidates, showing improved conversion of *N*-benzylpyrrolidine and *N*-benzylpiperidine. Notably, mutants from I177, V212, I213, and A241 significantly boosted conversions. The best-performing mutant for *N*-benzylpyrrolidine, *Mes*IRED$^{V212A/I213V}$ (M1), increased conversion from 23.7% to 74.3%. For *N*-benzylpiperidine, *Mes*IRED$^{V212A/I177A/A241I}$ (M2) enhanced conversion from 22.8% to 66.8%. Tunnel analysis revealed M1 and M2 have more efficient tunnels for larger product movement compared to wild-type *Mes*IRED. Using recombinant *E. coli* coexpressing *Mes*IRED and glucose dehydrogenase (GDH), high conversions were achieved: 75.1% for *N*-benzylpyrrolidine (M1) and 88.8% for *N*-benzylpiperidine (M2). A preparative experiment resulted in 86.2% conversion and 60.2% yield for *N*-benzylpiperidine. This research offers an efficient method for engineering IRED, significantly improving conversion and selectivity for *N*-benzyl cyclo-tertiary amines, aiding drug synthesis and providing insights into rational design of other enzymes.

Keywords: imine reductase; *N*-benzyl cyclo-tertiary amines; alanine scanning; consensus mutation; whole-cell biocatalysis; coexpression

check for updates

Citation: Zhang, Z.-H.; Wang, A.-Q.; Ma, B.-D.; Xu, Y. Rational Engineering of *Mesorhizobium* Imine Reductase for Improved Synthesis of *N*-Benzyl Cyclo-tertiary Amines. *Catalysts* **2024**, *14*, 23. https://doi.org/10.3390/catal14010023

Academic Editors: Jing Zhao and Jiandong Zhang

Received: 10 December 2023
Revised: 23 December 2023
Accepted: 26 December 2023
Published: 27 December 2023

Copyright: © 2023 by the authors. Licensee MDPI, Basel, Switzerland. This article is an open access article distributed under the terms and conditions of the Creative Commons Attribution (CC BY) license (https://creativecommons.org/licenses/by/4.0/).

1. Introduction

N-benzyl cyclo-tertiary amines are basic building blocks of many active pharmaceutical ingredients, such as donepezil [1] and trimetazidine [2] (Figure 1). Developing efficient pathways that allow for the synthesis of *N*-benzyl tertiary amines, especially starting from *N*-cyclic secondary amines, is an attractive route.

Furthermore, the catalytic reductive amination of carbonyl compounds and secondary amines, facilitated by transition metals and hydrosilatrane, has made notable contributions to the synthesis of *N*-benzyl cyclo-tertiary amines [3–5]. This process offers an efficient way to access tertiary amines, as illustrated in Scheme 1.

In contrast to traditional chemical methods, biocatalysis presents a green alternative. Enzymes derived from nature, following directed engineering, can catalyze the reductive amination more mildly and efficiently under aqueous conditions [6–8]. This highlights the potential of biocatalysis as a sustainable and effective approach in the synthesis of *N*-benzyl cyclo-tertiary amines.

It is fascinating to see the progress made in identifying enzymes capable of catalyzing the amination of carbonyl compounds. Among these enzymes, transaminases (TAs) [9], amine dehydrogenases (AmDHs) [10], and imine reductases (IREDs) [11] have shown promise. While TAs and AmDHs are limited to primary amines, IREDs, such as the NADPH-dependent reductive aminase (*Asp*RedAm) from *Aspergillus oryzae*, have the

ability to catalyze the reduction of prochiral imines to chiral amines using NAD(P)H as a cofactor. This enzyme can accept both primary and secondary amines as substrates for reductive amination reactions, making it highly versatile [12]. Currently, the fungal *Asp*RedAm is produced mainly as inclusion bodies in *E. coli*, which restricts its synthetic application [8].

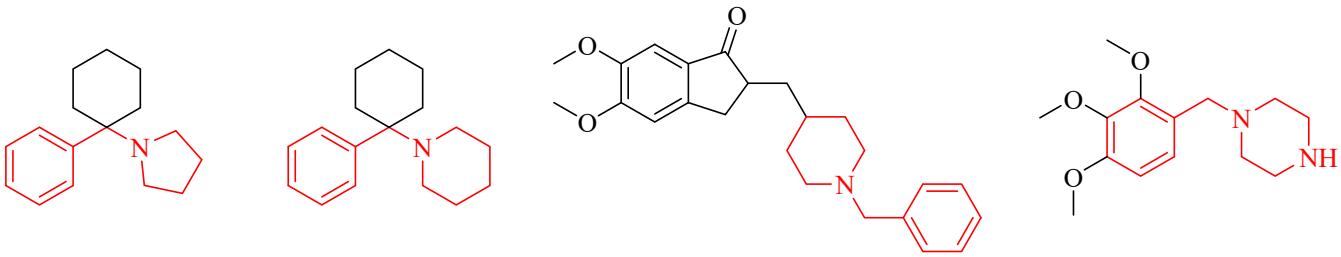
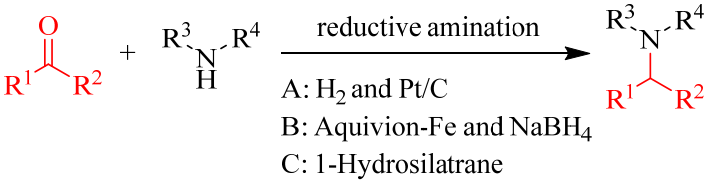
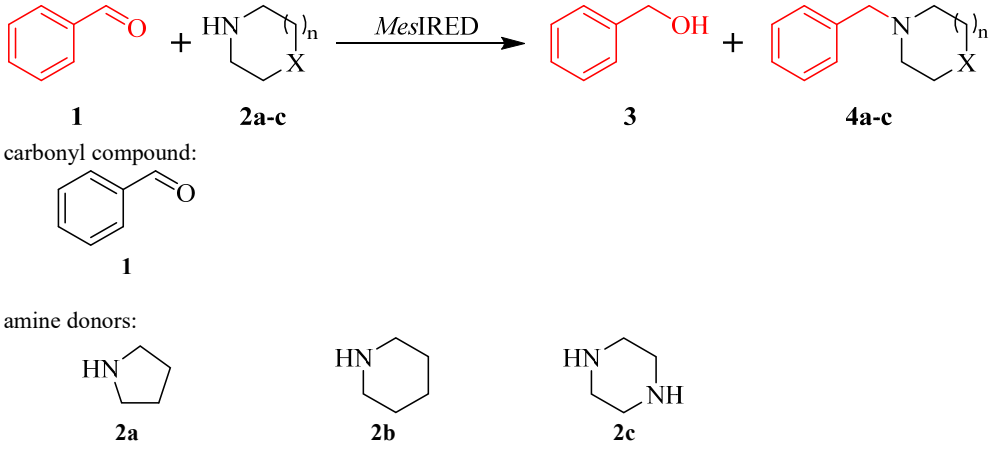


Figure 1. Bioactive compounds that are based on *N*-Benzyl cyclo-tertiary amines as building blocks.



Scheme 1. Comparison of synthetic pathways to access benzylaminie derivatives: (**A**) direct reductive amination using hydrogen gas and Pt/C as a heterogeneous catalyst; (**B**) one-pot reductive aminations with aquivion-Fe and sodium borohydride as catalyst; (**C**) metal-free direct reductive amination using hydrosilatrane as catalyst.

Researchers, led by Turner et al., have also identified a group of bacterial IREDs with great potential. One such enzyme, an imine reductase from *Mesorhizobium* sp. (*Mes*IRED), has been found to efficiently catalyze the reductive amination of cyclohexanone and pyrrolidine to *N*-cyclohexylpyrrolidine. This reaction achieved a high conversion rate of over 99% and an isolated yield of 71% [13]. Currently, the wild-type *Mes*IRED has limitations in accepting aldehyde substrates and tends to produce alcohol byproducts. However, the researchers believe that by engineering *Mes*IRED, they can develop a biosynthetic pathway for *N*-benzyl cyclo-tertiary amines in high yield (Scheme 2).



Scheme 2. Reductive amination benzaldehyde and *N*-heterocycle substrate panel for *Mes*IRED mutants screening.

NADPH serves as a stoichiometric equivalent in the catalytic reductive amination process mediated by *Mes*IRED, an NADPH-dependent oxidoreductase [14,15]. However, NAD(P)H is expensive and cannot be easily supplemented externally. Therefore, in laboratory settings, NAD(P)H is typically regenerated by coupling it with another oxidoreductase, which sacrifices a cosubstrate [16]. One common approach for NAD(P)H regeneration is to utilize glucose dehydrogenase (GDH) and glucose. This strategy is cost-effective, highly efficient, and stable. Additionally, the hydrolysis of gluconolactone, a coproduct, to gluconic acid makes this process nearly irreversible, thereby providing a strong driving force for NAD(P)H regeneration [17].

To eliminate the need for nonessential cofactors, we constructed recombinant cells coexpressing *Mes*IRED and GDH, enabling the expression of both enzymes within a single cell for biotransformation. This whole-cell catalysis strategy is gaining popularity due to its ability to bypass enzyme extraction and purification, while offering mild conditions for biocatalysis [18]. Moreover, the presence of intracellular membrane systems and cytoskeleton enhances the efficiency of collaborative multienzyme reactions [19].

In this paper, rational design methods were employed to address the issue of low activity and selectivity in wild-type *Mes*IRED for the synthesis of *N*-benzyl cyclo-tertiary amines, with a particular focus on the region surrounding the active pocket of the enzyme. Recombinant *E. coli* containing the optimal mutants of *Mes*IRED and GDH were constructed. Furthermore, the utilization of whole-cell biocatalyst coexpressing *Mes*IRED and GDH was applied for the synthesis of *N*-benzyl cyclo-tertiary amines.

2. Results

2.1. Selection of Mutation Sites Based on Alanine Scanning and Consensus Mutagenesis

Two strategies were used for selection of mutation sites for *Mes*IRED engineering: one is the alanine scanning of *Mes*IRED active pocket and another is consensus mutagenesis. For alanine scanning, the protein model of *Mes*IRED was modeled based on AlphaFold2 and the crystal structure of *Asp*RedAm (PDB: 5G6S). The *Mes*IRED folding pattern was supposed to be a conserved homodimeric structure. The model of *Mes*IRED suggests that the monomer comprises an N-terminal Rossman domain for NADP(H) binding, which is connected to a C-terminal helical bundle by a long helix (Figure 2A) [20]. The docking results of *N*-benzylpyrrolidine (**4a**), *N*-benzylpiperidine (**4b**), and *N*-benzylpiperazine (**4c**) with *Mes*IRED are shown in Figure 2C–E, respectively. The simple structure and low steric hindrance of alanine result in minimal impact on the overall protein structure. Therefore, 10 residues surrounding the active pocket were designed to be mutated to alanine.

Consensus mutagenesis was conducted according to the MSA method. By blasting the amino acid sequence of *Mes*IRED in NCBI and analyzing residue frequencies, a total of 13 conserved but different (CbD) single-site mutants (Figure 2B) were identified from 23 sites around the active pocket [21]. All these selected single-mutants were constructed by overlap extension PCR for further experimental examination for their synthetic ability of **4a**–**c**.

2.2. Biosynthesis of N-Benzyl Cyclo-tertiary Amines Conducted by MesIRED Mutants with Improved Conversion

All 23 mutants were tested for their ability to catalyze the reduction of benzaldehyde or the reductive amination of benzaldehyde with pyrrolidine, piperidine, and piperazine. The wild-type and single-site mutants of *Mes*IRED showed good alcohol dehydrogenase (ADH) activity on the synthesis of benzyl alcohol when using benzaldehyde as the sole substrate. However, they showed different IRED and ADH activity when using benzaldehyde and different *N*-cyclic secondary amines as substrates (Table S1). In this study, we focused on the role of residues in the pocket that are responsible for catalyzing the reductive amination reaction. Through alanine scanning experiments on residues M121, D171, L174, L175, I177, M178, T209, V212, I213, and L216, we found that three mutants (Table 1, M121A, D171A, and L175A) lost their ability to catalyze the reductive amination reaction while

maintaining alcohol dehydrogenase (ADH) activity [22]. These results indicate the critical nature of these residues in completing the reductive amination reaction. In contrast, the I177A and V212A mutants showed significant increases in the conversion of **4a** and **4b** (Table 1). Among the 13 mutants obtained through consensus mutations, some mutants demonstrate heightened conversions for **4a** and **4b**. In particular, the conversion of **4b** exhibited a significant increase, especially for the T209L and V212G mutants. The E507Q and E734N mutants of DNA polymerase, identified through consensus mutation, also exhibited remarkable enhancements in both activity and stability [23].

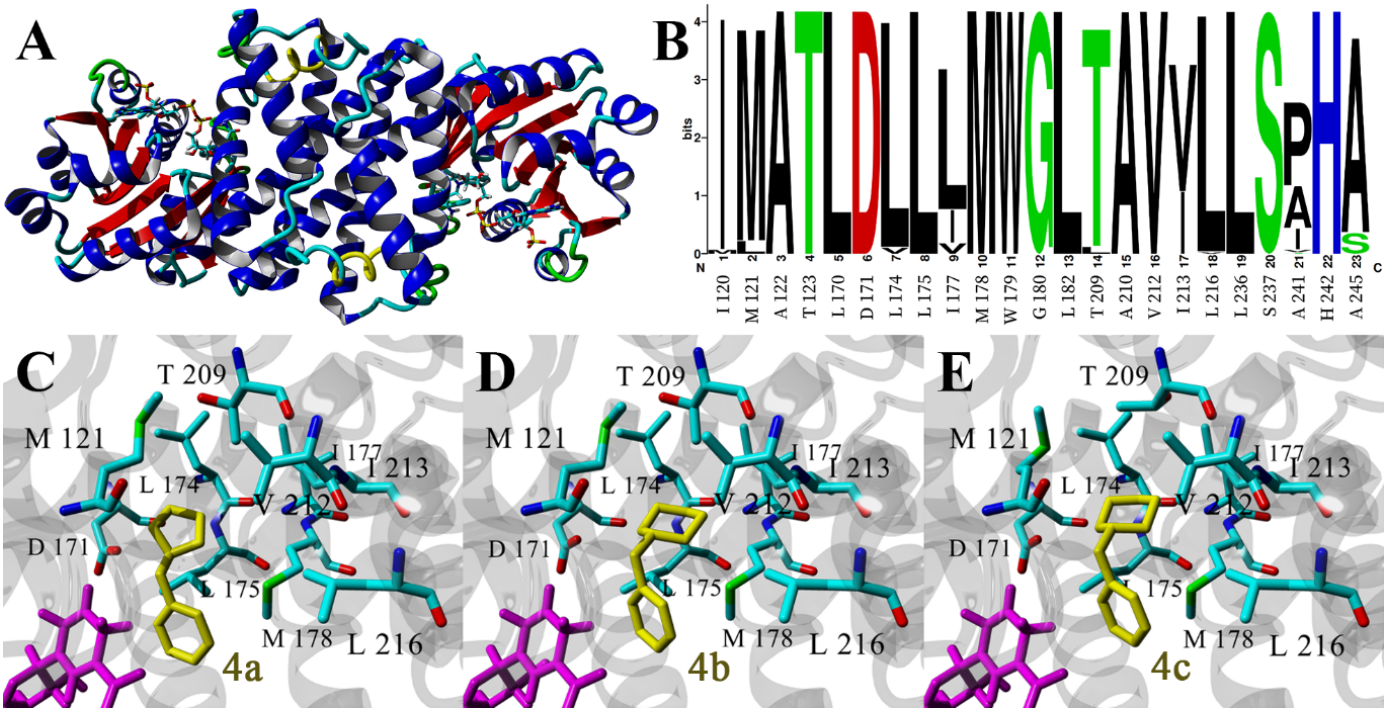
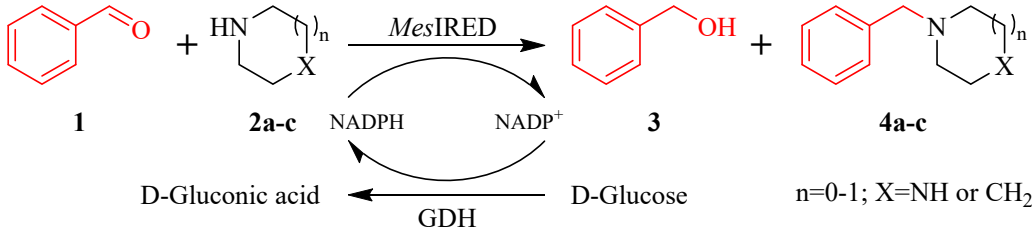


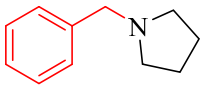
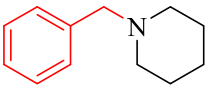
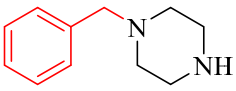
Figure 2. (**A**) Three-dimensional homodimeric model of *Mes*IRED in complex with cofactor NADPH. (**B**) Sequence logo generated by alignment of 100 IREDs (BLAST results with *Mes*IRED as template). (**C**) The docking model of *N*-benzylpyrrolidine (**4a**) and NADPH with *Mes*IRED active pocket. (**D**) The docking model of *N*-benzylpiperidine (**4b**) and NADPH with *Mes*IRED active pocket. (**E**) The docking model of *N*-benzylpiperazine (**4c**) and NADPH with *Mes*IRED active pocket. *N*-benzyl cyclo-tertiary amines are shown in yellow and NADPH is shown in purple.

In the initial screening for single mutants, positive mutants for catalytic synthesis of both *N*-benzylpyrrolidine and *N*-benzylpiperidine were identified, but unfortunately, no mutants that accepted piperazine were discovered by using these two strategies. It can be seen from Table 1 that the mutant T209L had the highest conversion of *N*-benzylpyrrolidine, while V212A had the highest conversion of *N*-benzylpiperidine, and M121L had the highest benzyl alcohol conversion in biotransformation of *N*-benzylpiperazine.

To uncover the untapped biocatalytic potential, further exploration of mutant combinations involved selecting the above-mentioned three mutants and combining them with other relevant positive sites. The biotransformation results of the dual-site mutants are shown in Table 2. Unfortunately, no mutants showed any activity on the synthesis of *N*-benzylpiperazine. Among them, the dual-site mutant *Mes*IRED V212A/I213V achieved the highest conversion for both *N*-benzylpyrrolidine and *N*-benzylpyridine, with conversion of 74.3% and 63.4%, respectively. It was 2.14 times and 2.78 times higher than that of the wild type, respectively. T209L/L216V and V212A/I177A were suboptimal dual-site mutants for the synthesis of *N*-benzylpyrrolidine and *N*-benzylpiperidine, respectively. Based on these three dual-site mutants, the next round of iterative combination mutations was carried out.

Table 1. Conversions of benzyl alcohol and *N*-benzyl cyclo-tertiary amines by wild-type and some positive single-site mutants of *Mes*IRED.



Strategy	Mutants	Conversion (%)		
				
		3, 4a	3, 4b	3, 4c
	WT	76.3, 23.7	77.2, 22.8	3.1, 0.0
Alanine scanning	M121A	>99.9, 0.0	93.9, 0.0	0.0, 0.0
	D171A	>99.9, 0.0	>99.9, 0.0	2.9, 0.0
	L175A	>99.9, 0.0	>99.9, 0.0	1.2, 0.0
	I177A	43.2, 56.8	62.2, 37.8	1.3, 0.0
	V212A	**40.8, 59.2**	54.7, 45.3	0.0, 0.0
Consensus mutagenesis	I120M	88.9, 11.1	82.4, 17.6	15.3, 0.0
	M121L	58.9, 41.1	77.6, 22.4	**32.0, 0.0**
	L174V	71.6, 28.4	78.6, 21.4	19.9, 0.0
	T209L	62.7, 37.3	**51.5, 48.5**	2.6, 0.0
	T209I	49.1, 50.9	52.3, 47.7	0.8, 0.0
	T209V	48.4, 51.6	63.8, 36.2	22.3, 0.0
	V212G	48.5, 51.5	51.7, 48.3	0.8, 0.0
	I213V	60.2, 39.8	72.6, 27.4	1.9, 0.0
	L216V	50.9, 49.1	69.1, 30.9	1.9, 0.0
	A241I	60.3, 39.7	63.1, 36.9	11.2, 0.0

Triple mutants were engineered by combining the double mutants V212A/I213V and T209L/L216V, as well as V212A/I177A, with individual mutations V212A, T209L, I177A, I213V, L216V, and A241I. The outcomes are delineated in Table 3. Post iterative recombination, the resultant triple mutants exhibited suboptimal performance; all except for the V212A/I177A/A241I variant demonstrated a decline in conversion rates. The V212A/I177A/A241I mutant manifested a marginal enhancement in the catalytic synthesis of *N*-benzylpiperidine. The diminution or loss of catalytic function in other variants is likely attributable to an excessive introduction of mutational sites, which presumably altered the conformation of the catalytic pocket, subsequently reducing the conversion efficiency of *N*-benzyl tertiary amines. Notably, the A241I mutation introduced in V212A/I177A/A241I is situated at a considerable distance from the active pocket, thus sparing the structural integrity of the catalytic site from significant alterations.

Despite two rounds of iterative combination mutation, no mutant capable of producing *N*-benzylpiperazine was identified. However, *Mes*IRED$^{V212A/I213V}$ and *Mes*IRED$^{V212A/I177A/A241I}$ were the best mutants for the synthesis of *N*-benzylpyrrolidine and *N*-benzylpiperidine, respectively.

Table 2. Conversions of benzyl alcohol and *N*-benzyl cyclo-tertiary amines by dual-site mutants of *Mes*IRED.

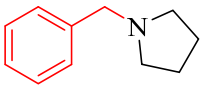
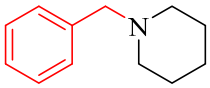
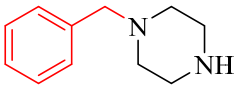
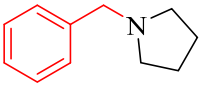
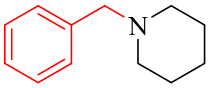
Strategy	Mutants	Conversion (%)		
				
		3, 4a	**3, 4b**	**3, 4c**
Combinatorial mutagenesis	T209L	62.7, 37.3	51.5, 48.5	2.6, 0.0
	T209L/I177A	83.2, 16.9	79.2, 20.8	13.2, 0.0
	T209L/V212A	51.6, 48.4	76.4, 23.6	15.4, 0.0
	T209L/V212G	76.2, 23.8	90.4, 9.6	21.2, 0.0
	T209L/I213V	80.3, 19.7	76.5, 23.6	0.5, 0.0
	T209L/L216V	**24.0, 72.2**	22.5, 37.9	6.0, 0.0
	T209L/A241I	45.6, 54.4	47.3, 52.8	17.4, 0.0
	V212A	40.8, 59.2	54.7, 45.3	0.0, 0.0
	V212A/I177A	33.6, 66.4	**41.8, 58.2**	29.6, 0.0
	V212A/T209I	27.1, 44.1	22.4, 24.8	6.1, 0.0
	V212A/T209V	36.0, 64.0	44.7, 55.3	16.7, 0.0
	V212A/I213V	**25.7, 74.3**	**36.6, 63.4**	11.5, 0.0
	V212A/L216V	44.0, 56.0	76.5, 23.5	41.1, 0.0
	V212A/A241I	41.1, 58.9	42.3, 57.7	30.7, 0.0
	M121L	58.9, 41.1	77.6, 22.4	32.0, 0.0
	M121L/I120M	49.4, 50.6	52.4, 47.6	30.2, 0.0
	M121L/L174V	42.2, 57.9	56.5, 43.5	23.0, 0.0
	M121L/T209V	43.6, 56.4	59.5, 40.5	24.9, 0.0
	M121L/A241V	53.0, 47.0	78.4, 21.6	28.5, 0.0

Table 3. Conversions of benzyl alcohol and *N*-benzyl cyclo-tertiary amines by triple-site mutants of *Mes*IRED.

Strategy	Mutants	Conversion (%)	
			
		3, 4a	**3, 4b**
Combinatorial mutagenesis	**V212A/I213V**	**25.7, 74.3**	36.6, 63.4
	V212A/I213V/I177A	2.2, 0.0	2.5, 0.0
	V212A/I213V/T209L	6.2, 0.0	9.5, 0.0
	V212A/I213V/L216V	9.1, 10.7	17.0, 0.0
	V212A/I213V/A241I	40.9, 59.1	44.7, 55.3
	T209L/L216V	24.0, 72.2	22.5, 37.9
	T209L/L216V/I177A	2.7, 0.0	3.8, 0.0
	T209L/L216V/V212A	11.0, 14.0	14.7, 9.0
	T209L/L216V/I213V	2.4, 0.0	2.9, 0.0
	T209L/L216V/A241I	50.4, 49.6	54.4, 45.6
	V212A/I177A	33.6, 66.4	41.8, 58.2
	V212A/I177A/T209L	22.8, 13.6	29.6, 0.0
	V212A/I177A/L216V	14.6, 14.1	18.1, 0.0
	V212A/I177A/A241I	38.6, 61.4	**35.2, 66.8**

2.3. Analyzing the Tunnels of Substrate and Product in MesIRED and Its Mutants

Building upon previous research into the catalytic mechanism of imine reductases, the catalytic process of *Mes*IRED is proposed to encompass the following steps: The cofactor NADPH, benzaldehyde, and *N*-secondary amine are sequentially bound to the active pocket. Subsequently, benzaldehyde and the *N*-secondary amine are activated by catalytic residues and are combined to form an iminium ion intermediate. This intermediate is then reduced by the NADPH cofactor, yielding the final product, *N*-benzyl cyclo-tertiary

amine. If the activated benzaldehyde is directly reduced by the NADPH cofactor, the by-product benzyl alcohol will be formed [11]. When the residue valine at site 212 in the catalytic pocket was mutated to alanine, both the conversions of *N*-benzylpyrrolidine and *N*-benzylpiperidine were increased. Pymol Caver 3.0 was used to analyze tunnel in *Mes*IRED, *Mes*IRED$^{V212A/I213V}$ (M1) and *Mes*IRED$^{V212A/I177A/A241I}$ (M2) [24]. It can be seen from Figure 3 that the interaction between V212A and other mutation sites collectively reshaped the entire tunnel, resulting in a reduction in length from 20.47 Å (wild-type *Mes*IRED, Figure 3A) to 17.76 Å (M1, Figure 3B) for *N*-benzylpyrrolidine and 22.32 Å (wild-type *Mes*IRED, Figure 3C) to 18.17 Å (M2, Figure 3D) for *N*-benzylpiperidine. This observation indicates that the tunnel of mutants from the active pocket to the surface becomes straighter and shorter. An increase in throughput from 0.59 (Figure 3A) to 0.68 (Figure 3B) and 0.57 (Figure 3C) to 0.65 (Figure 3D) was found based on Pymol Caver 3.0 tunnel analysis. The new tunnels will accelerate the exchange efficiency for larger products, which may be one of the reasons for improved conversion of *N*-benzyl cyclo-tertiary amines by M1 and M2. These results suggest that the V212A mutation plays significant role, despite not directly participating in the reductive amination.

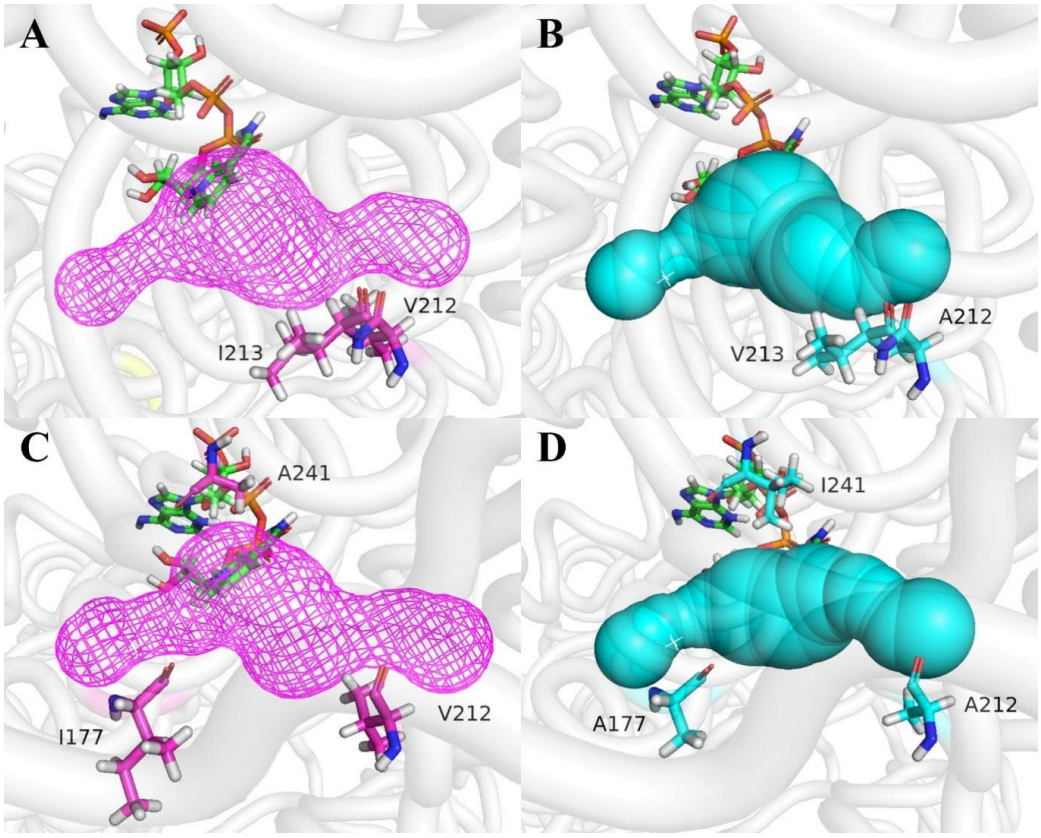


Figure 3. Tunnel analysis results after docking *N*-benzylpyrrolidine to WT (**A**) and M1 (**B**) and *N*-benzylpiperidine to WT (**C**) and M2 (**D**). The tunnels of WT are depicted using a purple mesh, and the mutated tunnels are shown in cyan. M1 and M2 are *Mes*IRED$^{V212/I213V}$ and *Mes*IRED$^{V212A/I177A/A241I}$, respectively.

2.4. Construction of E. coli Coexpressing IRED and GDH

To improve the efficiency of biotransformation, we developed a whole-cell reaction system illustrated in Figure 4, using the plasmid pRSFDuet1 to coexpress *Mes*IRED, *Mes*IRED$^{V212/I213V}$, and *Mes*IRED$^{V212A/I177A/A241I}$ with GDH in *E. coli* BL21 Gold (DE3). The molecular weight of *Mes*IRED is about 31.0 KDa, while that of GDH is about 28.1 KDa. However, due to addition of the His-Tag at the N-terminal of GDH during plasmid construction, the actual molecular weight of GDH is about 29.7 KDa. Although we increased the gel

to 15%, the small difference of 1.3 KDa in molecular weight between the two enzymes still makes it challenging to separate them into distinct bands during SDS-PAGE (Figure S1). Nevertheless, *Mes*IRED activity of 374.6 U/L, *Mes*IRED$^{V212/I213V}$ activity of 212.2 U/L, *Mes*IRED$^{V212A/I177A/A241I}$ activity of 207.4 U/L, and GDH activity of 1109.3 U/L were detected in the cell-free extract (Figure S2), indicating that IRED and GDH were successfully coexpressed in the recombinant *E. coli* after IPTG induction.

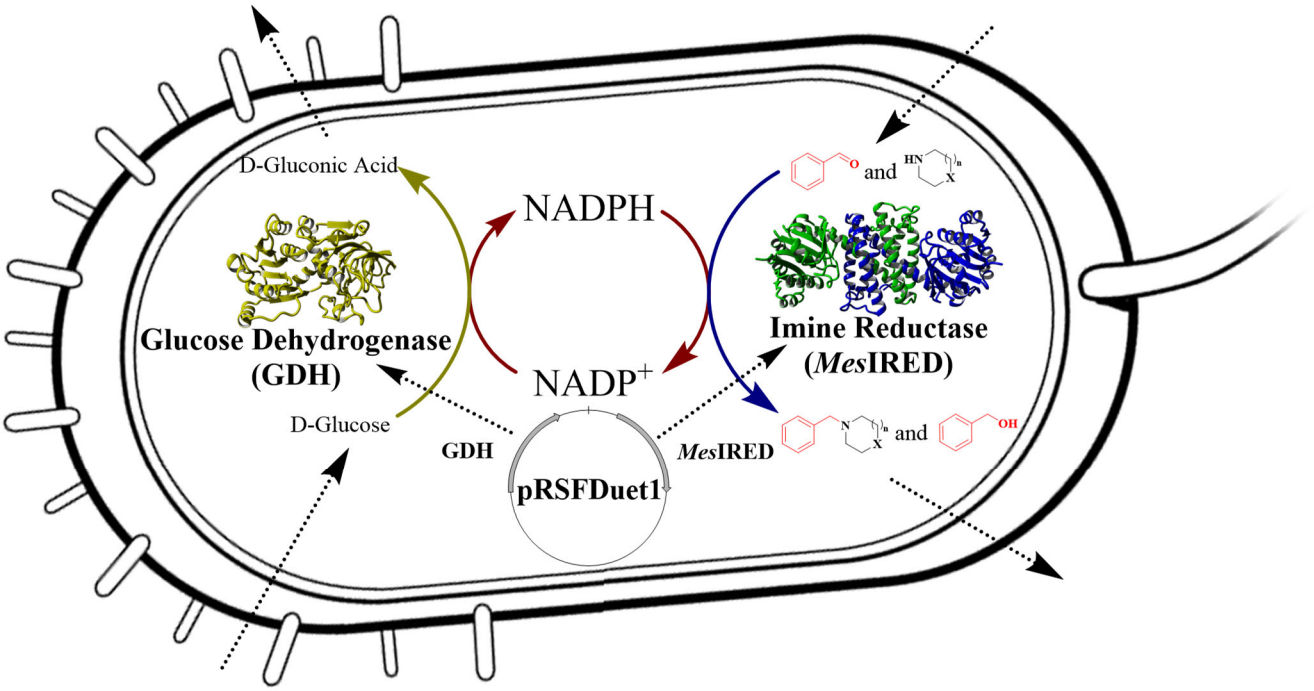


Figure 4. Biocatalytic synthesis of *N*-benzyl cyclic tertiary amines by whole cells coexpressing IRED and GDH.

2.5. Optimizing the Biotransformation for N-benzyl Cyclo-tertiary Amines Synthesis by Whole Cells

The reaction conditions for the conversions of *N*-benzylpyrrolidine (**4a**) and *N*-benzylpiperidine (**4b**) by whole cells of recombinant *E. coli* coexpressing *Mes*IRED and GDH were explored. It was found that temperature (Figures S3 and S4) and cell amount (Figures S5 and S6) play important roles on the conversion of **4a** and **4b**. The cofactor NADP$^+$ also contributes to the conversion of *N*-benzyl cyclo-tertiary amines (Table 4, Entry 1–3; Table 5, Entry 1–3). The appropriate conditions for biotransformation reaction were explored, partial results can be found in Tables 4 and 5. After 24 h of reaction, the conversions of **4a** and **4b** were 26.0% and 24.5%, respectively, at 5 mM of benzaldehyde (Table 4, Entry 4; Table 5, Entry 2).

In whole-cell catalytic reactions, **4a** and **4b** can be efficiently synthesized at a biomass of 10 g/L, with conversions of 67.2% and 76.0%, respectively (Table 4, Entry 7; Table 5, Entry 8). Based on the current best reaction conditions, optimization of substrate concentration was conducted. It was observed that a high concentration of pyrrolidine had a significant negative impact on enzyme activity (Table 4, Entry 11). Therefore, the optimal concentrations of benzaldehyde and pyrrolidine are 10 mM and 20 mM, and the conversion of **4a** reached 73.7% at 8 h and 75.1% at 24 h (Table 4, Entry 9 and 10). At the same time, the optimal concentration of benzaldehyde and piperidine is 20 mM and 400 mM, and the conversion of **4b** reached 83.8% at 8 h and 88.8% at 24 h (Table 5, Entry 11 and 12).

Table 4. Biocatalytic synthesis of **4a** by whole cells of *E. coli* coexpressing *Mes*IREDs and GDH under different conditions.

Entry	IREDs	1 (mM)	2a (mM)	$NADP^+$ (mM)	Biomass (g/L)	Time (h)	Conv. (%)
1	WT	5	10	0	5	24	15.7
2	WT	5	10	0.1	5	24	15.9
3	WT	5	10	0.5	5	24	22.4
4	WT	5	10	0.5	10	24	26.0
5	WT	10	20	0.5	10	24	16.1
6	M1	5	10	0.5	5	24	50.3
7	M1	5	10	0.5	10	24	67.2
8	M1	5	10	0.5	20	24	63.5
9	M1	10	20	0.5	10	8	73.7
10	M1	10	20	0.5	10	24	75.1
11	M1	20	40	0.5	10	24	1.6

Initial reaction conditions: coexpression cells as catalysts, 100 mM pH 9.0 Tris-HCl buffer, 30 mM D-glucose, and 2% DMSO in a total volume of 1000 µL. The reaction was incubated at 25 °C with shaking at 1000 rpm for 24 h. WT: *Mes*IRED; M1: *Mes*IRED$^{V212/I213V}$.

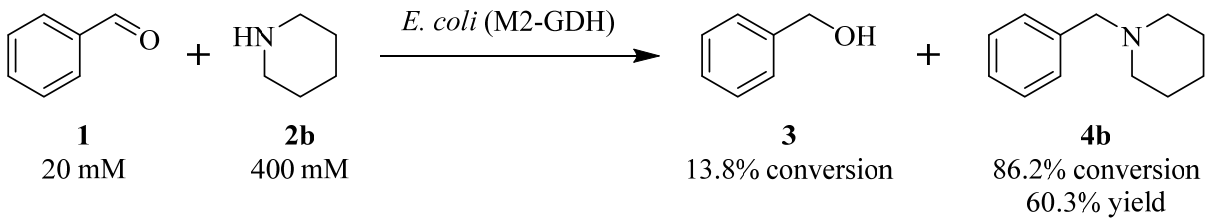
Table 5. Biocatalytic synthesis of **4b** by whole cells of *E. coli* coexpressing *Mes*IREDs and GDH under different conditions.

Entry	IREDs	1 (mM)	2b (mM)	$NADP^+$ (mM)	Biomass (g/L)	Time (h)	Conv. (%)
1	WT	5	100	0	5	24	21.1
2	WT	5	100	0.1	5	24	24.5
3	WT	5	100	0.5	5	24	24.8
4	WT	10	200	0.1	10	24	39.3
5	WT	20	400	0.1	10	24	25.5
6	WT	5	100	0.1	5	24	24.5
7	M2	5	100	0.1	5	24	72.1
8	M2	5	100	0.1	10	24	76.0
9	M2	5	100	0.1	20	24	76.3
10	M2	10	200	0.1	10	24	84.4
11	M2	20	400	0.1	10	8	83.8
12	M2	20	400	0.1	10	24	88.8

Initial reaction conditions: coexpression cells as catalysts, 100 mM pH 9.0 Tris-HCl buffer, 30 mM D-glucose, and 2% DMSO in a total volume of 1000 µL. The reaction was incubated at 25 °C with shaking at 1000 rpm for 24 h. WT: *Mes*IRED; M2: *Mes*IRED$^{V212A/I177A/A241I}$.

2.6. Preparative Scale of N-Benzylpiperidine Using Whole Cells

To test the synthetic applicability of whole cells containing IRED and GDH, a preparative-scale reaction was performed. Taking **1** and **2b** as model substrates, the optimal reaction conditions (Table 5, Entry 12) were selected at a 50 mL reaction volume for biocatalytic synthesis of **4b** by whole cells coexpressing M2 and GDH. It can be seen from Figure 5 that the conversion of **4b** reached 84.3% at 8 h and was 86.2% after 24 h reaction. After separation and purification, 105.8 mg of pure **4b** was obtained as colorless oil in 60.3% isolated yield (Scheme 3). The purity and quality of **4b** was verified by GC (Figure S7) and NMR (Figure S8).



Scheme 3. Biocatalytic synthesis of **4b** by whole cells of *E. coli* (M2-GDH) on preparative scale.

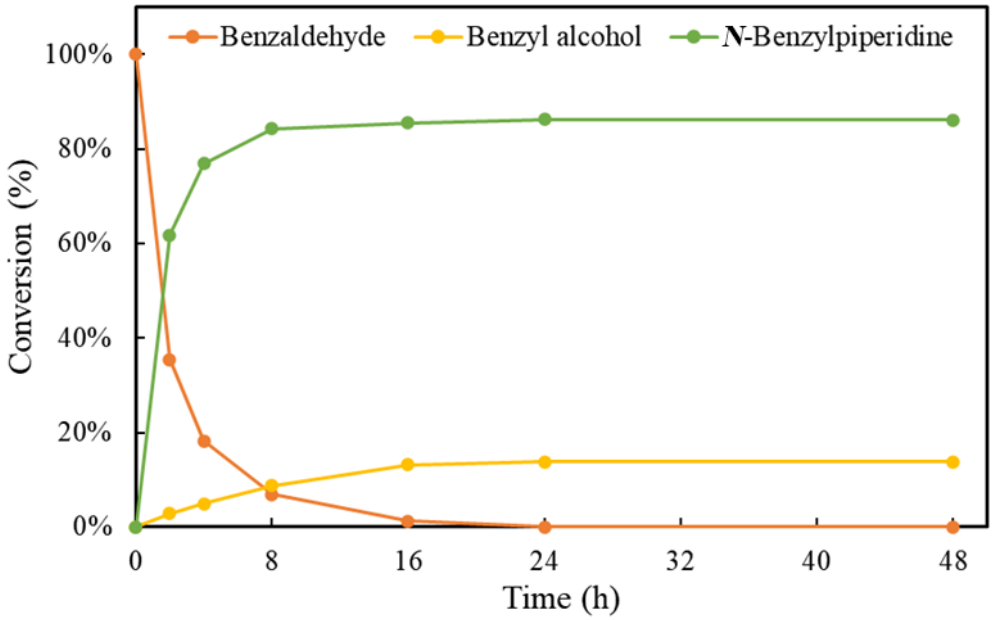


Figure 5. Time courses on whole-cell biocatalytic synthesis of **4b** by *E. coli* (M2-GDH).

3. Discussion

In the current study, rational engineering of *Mes*IRED and the construction of whole-cell biocatalysts coexpressing IRED and GDH enabled the green manufacturing of *N*-benzyl cyclo-tertiary amines with good yield. Our findings provide valuable insights into the mechanisms underlying this reaction, which can help to optimize and tailor it for various applications. The preparative biotransformation displays substrate concentration of 20 mM, with the conversion up to 86.2%, which was much higher than that of the WT. The advantage of this work is to minimize the laborious IRED-engineering efforts by utilizing two rational strategies based on structural and sequence analysis. M1 and M2 were obtained through iterative combination mutations. The future engineering of *Mesorhizobium* imine reductase may adopt other rational design methods, such as energy-based rational strategies or combinations with artificial intelligence methods, to further improve enzyme activity and chemical selectivity and reduce the content of by-products.

4. Materials and Methods

4.1. Chemicals, Strains, and Plasmids

Commercially available chemicals and reagents were purchased from Macklin (Shanghai, China), Aladdin (Shanghai, China), Takara (Dalian, China), Tiangen (Beijing, China), Collins (Shanghai, China), Meryer (Shanghai, China), Sangon Biotech (Shanghai, China), Sinopharm (Shanghai, China), or Adamas (Shanghai, China), unless stated otherwise. *E. coli* BL21 Gold (DE3) was utilized as a host for heterologous expression of *Mes*IRED and coexpression of *Mes*IRED-GDH. *E. coli* BL21 (DE3) was utilized as a host for heterologous expression of GDH. Plasmids pET21a, pET28b, pRSFDuet1 from the Generay (Shanghai, China) were preserved in Biocatalysis and Biopharmaceutical laboratory (Shanghai Institute of Technology, Shanghai, China). The codon-optimized genes encoding the *Mes*IRED (accession no. WP_023809753.1) and GDH (accession no. WP_033578120.1) were synthesized by Generay Co. (Shanghai, China) and were incorporated into the vector pET28b (*Mes*IRED, *Nde* I and *Xho* I were restriction sites) and pET21a (GDH, *Bam*H I and *Hin*d III were restriction sites). The plasmids pET28b-*Mes*IRED and pRSFDuet1 were digested by *Nde* I and *Xho* I, and the target fragments were recovered and ligated overnight at 4 °C using DNA Ligation Kit (Takara Biotechnology, Dalian, China) to construct pRSFDuet1-*Mes*IRED. The plasmids pET21a-GDH and pRSFDuet1- *Mes*IRED were digested by *Bam*H I and *Hin*d III, and the target fragments were recovered and ligated overnight at 4 °C using DNA Ligation Kit to construct pRSFDuet1-*Mes*IRED-GDH (Table 6). The recombinant plasmids

pET28b-*Mes*IRED and pRSFDuet1-*Mes*IRED-GDH were chemically transformed into *E. coli* BL21 Gold (DE3) competent cells, respectively, while the pET21a-GDH was chemically transformed into *E. coli* BL21 (DE3) competent cells. All strains were preserved at −80 °C prior to use.

Table 6. Plasmids and genes used for the construction of strains.

Strains	Plasmids	Genes	Restriction Sites
E. coli BL21 Gold (DE3)	pET28b	*Mes*IRED	*Nde* I and *Xho* I
E. coli BL21 (DE3)	pET21a	GDH	*Bam*H I and *Hin*d III
E. coli BL21 Gold (DE3)	pRSFDuet1	*Mes*IRED GDH	*Nde* I and *Xho* I *Bam*H I and *Hin*d III

4.2. Prediction of Potential Active Variants and Site-Directed Mutagenesis

The prediction model for *Mes*IRED was constructed using AlphaFold2 (version 2.3.2, DeepMind, London, UK, 2023) on the Beikunyun high-performance computing platform (Shenzhen, China) [25]. The quality of the model was validated using PROCHECK (https://saves.mbi.ucla.edu/, accessed on 10 December 2023) [26,27] and ProSA (https://prosa.services.came.sbg.ac.at/prosa.php, accessed on 10 December 2023) [28,29]. Docking of the NADPH cofactor, product *N*-benzyl cyclo-tertiary amines into prediction model of *Mes*IRED was performed using dock_run script in the YASARA Structure (version 22.5.22, YASARA Biosciences GmbH, Vienna, Austria, 2022) [30]. A BLAST search on NCBI was performed to access the homologous IRED sequences, using *Mes*IRED sequence as the template. MSA was performed to obtain a consensus residue for *Mes*IRED using T-Coffee (protein structural alignments, Expresso, https://tcoffee.crg.eu/, accessed on 10 December 2023) [31]. Amino acid residues around the active pocket under selection were graphically visualized using WebLogo (https://weblogo.berkeley.edu/, accessed on 10 December 2023) [32].

A site-directed mutagenesis library was constructed through overlap extension PCR using primers (Table S2) that contained mutation codons. All transformed mutants were plated at a single colony density on LB agar plates containing 50 μg/mL kanamycin and were incubated overnight at 37 °C. Subsequently, single colonies were selected and confirmed by sequencing.

4.3. Cell Culture, Expression, and Enzyme Activity Assay of MesIRED and GDH

4.3.1. Cell Culture and Expression of MesIRED and MesIRED-GDH

A single colony of *E. coli* BL21 Gold (DE3) (bearing pET28b-*Mes*IRED or pRSFDuet1-*Mes*IRED-GDH) picked from a lysogeny broth (LB) agar plate (1% tryptone, 0.5% yeast extract, 1% NaCl, 1.5% agar powder) grown overnight was inoculated into 50 mL LB medium with 50 μg/mL kanamycin and incubated overnight at 37 °C with shaking at 200 rpm. The starter culture was used as the inoculum for a 50 mL culture in 2 × YT media (1.6% tryptone, 1.5% yeast extract, 0.5% NaCl) with 50 μg/mL kanamycin at 37 °C with shaking at 250 rpm. At OD_{600} between 0.6 and 0.8, isopropyl-β-D-thiogalactopyranoside (IPTG) was added to a final concentration of 0.5 mM to induce protein expression. Incubation was continued at 20 °C and 250 rpm for 18 h [12].

The cells were then harvested and suspended in 100 mM Tris-HCl buffer (pH 9.0) buffer. The cell suspensions (10 g_{dcw}/L) were disrupted twice using an ultra-pressure homogenizer (JNBIO, Guangzhou, China). Centrifugation was used to remove cell debris for 10 min at 12,000 rpm and 4 °C. The expressions of *Mes*IRED and GDH were verified by SDS-PAGE. Protein concentration was determined using the Bradford assay and a BSA standard curve.

4.3.2. Cell Culture and Expression of GDH

The same method was used to pick single colony of *E. coli* BL21 (DE3) (bearing pET21a-GDH) inoculation in the 50 mL LB medium with 100 μg/mL ampicillin and incubated

overnight at 37 °C with shaking at 200 rpm. The starter culture was used as the inoculum for a 50 mL culture in LB medium with 100 μg/mL ampicillin at 37 °C with shaking at 200 rpm. At OD_{600} between 0.6 and 0.8, IPTG was added to a final concentration of 0.1 mM to induce protein expression. Incubation was continued at 20 °C and 200 rpm for 20 h.

The cells were then harvested and suspended in 100 mM Tris-HCl buffer (pH 9.0) buffer. The cell suspensions (5 g_{dcw}/L) were disrupted twice using an ultra-pressure homogenizer (JNBIO, Guangzhou, China). Centrifugation was used to remove cell debris for 10 min at 12,000 rpm and 4 °C. The expression of GDH was verified by SDS-PAGE. Determine protein concentration by using the Bradford assay and a BSA standard curve.

4.3.3. Enzyme Activity Assay of MesIRED and GDH

*Mes*IRED activity assay: The reaction system was composed of 100 mM Tris-HCl buffer (pH 9.0), 15 mM cyclohexanone, 60 mM methylamine, 0.3 mM NADPH, 2% dimethylsulfoxide (*v*/*v*, DMSO) and an appropriate amount of cell-free extract, with a total volume of 1000 μL. One unit of *Mes*IRED activity is defined as the amount of enzyme catalyzing the consumption of 1 μmol NADPH per minute at 25 °C and pH 9.0. Activity measurement was performed at 340 nm (ε = 6.22 $mM^{-1}cm^{-1}$) for 5 min using a BioTek microplate reader (Agilent, Santa Clara, CA, USA).

GDH activity assay: The reaction system was composed of 100 mM Tris-HCl buffer (pH 9.0), 200 mM glucose, 0.2 mM $NADP^+$, 2% dimethylsulfoxide (*v*/*v*, DMSO) and an appropriate amount of cell-free extract, with a total volume of 1000 μL. One unit of GDH activity is defined as the amount of enzyme catalyzing the production of 1 μmol NADPH per minute at 25 °C and pH 9.0. Activity measurements were performed at 340 nm (ε = 6.22 $mM^{-1}cm^{-1}$) for 5 min using a BioTek microplate reader.

4.4. The Reductive Amination of Benzaldehyde with N-Cyclic Secondary Amines by MesIRED

The reductive amination reaction was conducted in a 100 mM Tris-HCl buffer at pH 9.0, containing cell-free extract (500 μL of *Mes*IRED, 100 μL of GDH) or coexpression cells (5 g/L of final concentration), 30 mM D-glucose, 1 mM $NADP^+$, 5 mM benzaldehyde, an appropriate ratio of cyclic secondary amines (2 eq. pyrrolidine, 20 eq. piperidine and piperazine), and 2% DMSO, with a total volume of 1000 μL [12]. The reaction mixture was incubated at 25 °C with shaking at 1000 rpm for 24 h. Then, reaction mixture was extracted with 2 mL of ethyl acetate containing 0.1% dodecane (internal standard). The organic fraction was dried over anhydrous $MgSO_4$, and analyzed by GC (GC-2010 plus, Shimadzu Co., Kyoto, Japan).

4.5. Determination of Benzaldehyde, Benzyl Alcohol, and N-Benzyl Cyclo-tertiary Amines

GC analysis was performed on a Shimadzu GC-2010 plus with a flame ionization detector (FID) (GC-2010, Shimadzu Co., Kyoto, Japan). Analysis was conducted on a SE-30 column (30 m × 0.32 mm × 0.25 μm film thickness, Zhonghuida, Dalian, China). Injector temperature: 200 °C, detector temperature: 250 °C, nitrogen flow 1.74 mL min^{-1}, split ratio 50.0, oven temperature: hold at 50 °C for 2 min, ramp from 50 to 200 °C at 10 °C min^{-1}, hold at 200 °C for 2 min. Retention times were assigned by comparison with compounds of known retention time. The retention time for benzaldehyde, benzyl alcohol, *N*-benzylpyrrolidine, and *N*-benzylpiperidine were 8.75 min, 10.13 min, 14.73 min, and 15.83 min, respectively.

4.6. Optimizing the Synthesis of N-Benzyl Cyclo-tertiary Amines by Whole Cells of E. coli (MesIRED-GDH), E. coli (M1-GDH) or E. coli (M2-GDH)

The initial reaction conditions were as follows: 5 g/L cells, 100 mM pH 9.0 Tris-HCl buffer, 30 mM D-glucose, 5 mM benzaldehyde, an appropriate ratio of *N*-cyclic secondary amines (2 eq. pyrrolidine, 20 eq. piperidine), $NADP^+$ concentration set as 0.5 mM (for **4a**) or 0.1 mM (for **4b**), and 2% DMSO in a total volume of 1000 μL. The reaction mixture was incubated in a Thermomixer at 25 °C and 1000 rpm for 24 h.

4.6.1. Optimization of Temperature

The reaction conditions were as follows: 5 g/L cells, 100 mM pH 9.0 Tris-HCl buffer, 30 mM D-glucose, 5 mM benzaldehyde, an appropriate ratio of cyclic secondary amines (2 eq. pyrrolidine, 20 eq. piperidine), and 2% DMSO in a total volume of 1000 μL. The reaction mixtures were incubated in a Thermomixer at different temperatures (15 °C, 20 °C, 25 °C, 30 °C, or 37 °C) and 1000 rpm for 24 h.

4.6.2. Optimization of $NADP^+$ Concentration

The reaction conditions were as follows: 5 g/L cells, 100 mM pH 9.0 Tris-HCl buffer, 30 mM D-glucose, 5 mM benzaldehyde, an appropriate ratio of cyclic secondary amines (2 eq. pyrrolidine, 20 eq. piperidine), and 2% DMSO in a total volume of 1000 μL. The NADP+ concentration was set as 0.0, 0.1, 0.5, 1.0, and 2.0 mM. The reaction mixtures were incubated in a Thermomixer at 25 °C and 1000 rpm for 24 h.

4.6.3. Optimization of Biomass

The reaction conditions were as follows: 100 mM pH 9.0 Tris-HCl buffer, 30 mM D-glucose, 5 mM benzaldehyde, an appropriate ratio of *N*-cyclic secondary amines (2 eq. pyrrolidine, 20 eq. piperidine), $NADP^+$ concentration set as 0.5 mM (for **4a**) or 0.1 mM (for **4b**), and 2% DMSO in a total volume of 1000 μL. The coexpression cell concentration was set as 1, 2, 5, 10, and 20 g/L. The reaction mixtures were incubated in a Thermomixer at 25 °C and 1000 rpm for 24 h.

4.6.4. Optimization of Substrate Concentration

The reaction conditions were as follows: 10 g/L cells, 100 mM pH 9.0 Tris-HCl buffer, $NADP^+$ concentration set as 0.5 mM (for **4a**) or 0.1 mM (for **4b**), and 2% DMSO in a total volume of 1000 μL. The benzaldehyde concentration was set as 5, 10, and 20 mM, and D-glucose is 6 eq., pyrrolidine is 2 eq., piperidine is 20 eq. of benzaldehyde. The reaction mixtures were incubated in a Thermomixer at 25 °C and 1000 rpm for 24 h.

4.7. Preparation of N-Benzylpiperidine by Whole Cells of E. coli (MesIRED-GDH)

The preparative reaction was performed in 100 mM pH 9.0 Tris-HCl buffer containing 10 g/L coexpressed cells, 20 mM benzaldehyde, 20 eq. piperidine, 6 eq. D-glucose, 0.5 mM $NADP^+$, and 2% DMSO in a total volume of 50 mL. The reaction mixture was incubated in 250 mL baffled flask at 25 °C and 250 rpm for 48 h. Samples were collected at 2 h, 4 h, 8 h, 16 h, 24 h, and 48 h during the reaction, and analyzed by GC. When the reaction finished, the reaction mixture was acidified to pH 2~3 with 6 M hydrochloric acid and then was extracted with ethyl acetate (3 × 50 mL) to remove the byproduct benzyl alcohol. Afterwards, the aqueous phase pH was adjusted to 10 by adding 6 M NaOH solution and the *N*-benzylpiperidine was extracted with ethyl acetate (3 × 50 mL). The combined organic phase was washed with saturated NaCl solution to remove DMSO and piperidine, and the organic phase was dried overnight with anhydrous Na_2SO_4. The dried ethyl acetate was evaporated under reduced pressure and pure *N*-benzylpiperidine was obtained as colorless liquid. The purity was analyzed by GC (Figure S7). The chemical structure was confirmed using nuclear magnetic resonance (NMR) ^{1}H NMR (400 MHz, $CDCl_3$): δ 7.37–7.21 (m, 5H), 3.52 (s, 2H), 2.44–2.41 (m, 4H), 1.65–1.46 (m, 6H). and ^{13}C NMR (100 MHz, $CDCl_3$): δ 138.62, 129.35, 128.18, 126.92, 63.98, 54.56, 26.04, 24.46. (Figure S8).

5. Conclusions

In this study, the active pocket of *Mes*IRED was rationally modified based on two rational strategies: alanine scanning and consensus mutation. A total of 12 positive single-site mutants of *Mes*IRED with improved conversion of *N*-benzylpyrrolidine or *N*-benzylpiperidine were identified from 23 candidate mutants. Further combination of these single mutants by iterative combination mutation provided the best multiple mutants, *Mes*IRED$^{V212A/I213V}$ (M1) for synthesizing *N*-benzylpyrrolidine and the best mutants

*Mes*IRED$^{V212A/I177A/A241I}$ (M2) for synthesizing *N*-benzylpiperidine. The tunnel analysis revealed that M1 and M2 have straighter and shorter tunnels than the wild-type *Mes*IRED, which are more conducive to the entry and exit of large product molecules. The recombinant *E. coli* coexpressing *Mes*IRED and glucose dehydrogenase (GDH) were constructed for the synthesis of *N*-benzyl cyclo-tertiary amines using whole cells as biocatalysts. Under optimal conditions, *N*-benzylpyrrolidine was obtained in 75.1% conversion by M1 and *N*-benzylpiperidine was obtained in 88.8% conversion by M2. In a preparative experiment, *N*-benzylpiperidine was prepared in 86.2% conversion and 60.2% yield. Our results exhibited a simple and efficient method for the rational engineering of IRED with significantly improved conversion and selectivity of *N*-benzyl cyclo-tertiary amines, which will contribute to the practical application of imine reductase in drug synthesis and also provide meaningful references for rational design of other enzymes.

Supplementary Materials: The following supporting information can be downloaded at: https://www.mdpi.com/article/10.3390/catal14010023/s1, Figure S1: SDS-PAGE assay of recombinant *Mes*IREDs and GDH; Figure S2: Enzyme activity determination of GDH, *Mes*IRED, and *Mes*IRED's mutants; Figure S3: Effect of temperature on the conversion of benzyl alcohol (left) and *N*-benzylpyrrolidine (right) by whole cells of *E. coli* (*Mes*IRED-GDH); Figure S4: Effect of temperature on the conversion of benzyl alcohol (left) and *N*-benzylpiperidine (right) by whole cells of *E. coli* (*Mes*IRED-GDH); Figure S5: Effect of cell amounts on the conversion of benzyl alcohol (left) and *N*-benzylpyrrolidine (right) by whole cells of *E. coli* (*Mes*IRED-GDH); Figure S6: Effect of cell amounts on the conversion of benzyl alcohol (left) and *N*-benzylpiperidine (right) by whole cells of *E. coli* (*Mes*IRED-GDH); Figure S7: The gas chromatograph of *N*-benzylpiperidine isolated from preparative-scale biotransformation; Figure S8: NMR spectrums of *N*-benzylpiperidine isolated from preparative-scale biotransformation; Table S1: Conversions of benzyl alcohol and *N*-benzyl cyclo-tertiary amines by wild-type and single-site mutants of *Mes*IRED; Table S2: Primers for site-directed mutangenesis.

Author Contributions: Conceptualization, Y.X.; methodology, B.-D.M. and Z.-H.Z.; validation, Z.-H.Z. and Y.X.; formal analysis, Z.-H.Z.; data curation, Z.-H.Z. and A.-Q.W.; writing—original draft preparation, Z.-H.Z.; writing—review and editing, B.-D.M. and Y.X.; funding acquisition, Y.X. All authors have read and agreed to the published version of the manuscript.

Funding: This research was funded by the Project of Leading Talents in Shandong Taishan Industry (Grant No. LJNY202019).

Data Availability Statement: Data are contained within the article.

Conflicts of Interest: The authors declare no conflicts of interest.

References

1. Kim, J.; Lee, H.J.; Park, S.K.; Park, J.H.; Jeong, H.R.; Lee, S.; Lee, H.; Seol, E.; Hoe, H.S. Donepezil Regulates LPS and Abeta-Stimulated Neuroinflammation through MAPK/NLRP3 Inflammasome/STAT3 Signaling. *Int. J. Mol. Sci.* **2021**, *22*, 10637. [CrossRef]
2. Borowicz-Reutt, K.; Banach, M. Trimetazidine, an Anti-Ischemic Drug, Reduces the Antielectroshock Effects of Certain First-Generation Antiepileptic Drugs. *Int. J. Mol. Sci.* **2022**, *23*, 11328. [CrossRef] [PubMed]
3. Airoldi, V.; Piccolo, O.; Roda, G.; Appiani, R.; Bavo, F.; Tassini, R.; Paganelli, S.; Arnoldi, S.; Pallavicini, M.; Bolchi, C. Efficient One-Pot Reductive Aminations of Carbonyl Compounds with Aquivion-Fe as a Recyclable Catalyst and Sodium Borohydride. *Eur. J. Org. Chem.* **2020**, *2020*, 162–168. [CrossRef]
4. Laroche, B.; Ishitani, H.; Kobayashi, S. Direct Reductive Amination of Carbonyl Compounds with H-2 Using Heterogeneous Catalysts in Continuous Flow as an Alternative to N-Alkylation with Alkyl Halides. *Adv. Synth. Catal.* **2018**, *360*, 4699–4704. [CrossRef]
5. Varjosaari, S.E.; Skrypai, V.; Suating, P.; Hurley, J.J.M.; De Lio, A.M.; Gilbert, T.M.; Adler, M.J. Simple Metal-Free Direct Reductive Amination Using Hydrosilatrane to Form Secondary and Tertiary Amines. *Adv. Synth. Catal.* **2017**, *359*, 1872–1878. [CrossRef]
6. Ming, H.; Yuan, B.; Qu, G.; Sun, Z.T. Engineering the activity of amine dehydrogenase in the asymmetric reductive amination of hydroxyl ketones. *Catal. Sci. Technol.* **2022**, *12*, 5952–5960. [CrossRef]
7. Zhang, J.; Li, X.; Chen, R.C.; Tan, X.W.; Liu, X.D.; Ma, Y.Q.; Zhu, F.F.; An, C.Y.; Wei, G.Z.; Yao, Y.P.; et al. Actinomycetes-derived imine reductases with a preference towards bulky amine substrates. *Commun. Chem.* **2022**, *5*, 123. [CrossRef] [PubMed]
8. Yang, Z.Y.; Hao, Y.C.; Hu, S.Q.; Zong, M.H.; Chen, Q.; Li, N. Direct Reductive Amination of Biobased Furans to N-Substituted Furfurylamines by Engineered Reductive Aminase. *Adv. Synth. Catal.* **2021**, *363*, 1033–1037. [CrossRef]

9. Patil, M.D.; Grogan, G.; Bommarius, A.; Yun, H. Recent Advances in omega-Transaminase-Mediated Biocatalysis for the Enantioselective Synthesis of Chiral Amines. *Catalysts* **2018**, *8*, 254. [CrossRef]
10. Knaus, T.; Bohmer, W.; Mutti, F.G. Amine dehydrogenases: Efficient biocatalysts for the reductive amination of carbonyl compounds. *Green Chem.* **2017**, *19*, 453–463. [CrossRef]
11. Sharma, M.; Mangas-Sanchez, J.; France, S.P.; Aleku, G.A.; Montgomery, S.L.; Ramsden, J.I.; Turner, N.J.; Grogan, G. A Mechanism for Reductive Amination Catalyzed by Fungal Reductive Aminases. *ACS Catal.* **2018**, *8*, 11534–11541. [CrossRef]
12. Aleku, G.A.; France, S.P.; Man, H.; Mangas-Sanchez, J.; Montgomery, S.L.; Sharma, M.; Leipold, F.; Hussain, S.; Grogan, G.; Turner, N.J. A reductive aminase from *Aspergillus oryzae*. *Nat. Chem.* **2017**, *9*, 961–969. [CrossRef] [PubMed]
13. France, S.P.; Howard, R.M.; Steflik, J.; Weise, N.J.; Mangas-Sanchez, J.; Montgomery, S.L.; Crook, R.; Kumar, R.; Turner, N.J. Identification of Novel Bacterial Members of the Imine Reductase Enzyme Family that Perform Reductive Amination. *ChemCatChem* **2018**, *10*, 510–514. [CrossRef]
14. Wang, X.D.; Saba, T.; Yiu, H.H.P.; Howe, R.F.; Anderson, J.A.; Shi, J.F. Cofactor NAD(P)H Regeneration Inspired by Heterogeneous Pathways. *Chem* **2017**, *2*, 621–654. [CrossRef]
15. Fukuzumi, S.; Lee, Y.M.; Nam, W. Catalytic recycling of NAD(P)H. *J. Inorg. Biochem.* **2019**, *199*, 110777. [CrossRef] [PubMed]
16. Han, L.; Liang, B. New approaches to NAD(P)H regeneration in the biosynthesis systems. *World J. Microbiol. Biotechnol.* **2018**, *34*, 141. [CrossRef] [PubMed]
17. Jeon, H.; Durairaj, P.; Lee, D.; Ahsan, M.M.; Yun, H. Improved NADPH Regeneration for Fungal Cytochrome P450 Monooxygenase by Co-Expressing Bacterial Glucose Dehydrogenase in Resting-Cell Biotransformation of Recombinant Yeast. *J. Microbiol. Biotechnol.* **2016**, *26*, 2076–2086. [CrossRef] [PubMed]
18. Patel, S.N.; Kaushal, G.; Singh, S.P. A Novel D-Allulose 3-Epimerase Gene from the Metagenome of a Thermal Aquatic Habitat and D-Allulose Production by *Bacillus subtilis* Whole-Cell Catalysis. *Appl. Environ. Microb.* **2020**, *86*, e02605-19. [CrossRef]
19. Wickstead, B.; Gull, K. The evolution of the cytoskeleton. *J. Cell Biol.* **2011**, *194*, 513–525. [CrossRef]
20. Mangas-Sanchez, J.; France, S.P.; Montgomery, S.L.; Aleku, G.A.; Man, H.; Sharma, M.; Ramsden, J.I.; Grogan, G.; Turner, N.J. Imine reductases (IREDs). *Curr. Opin. Chem. Biol.* **2017**, *37*, 19–25. [CrossRef]
21. Yu, H.; Ma, S.; Li, Y.; Dalby, P.A. Hot spots-making directed evolution easier. *Biotechnol. Adv.* **2022**, *56*, 107926. [CrossRef] [PubMed]
22. Wada, M.; Hayashi, Y.; Arai, M. Mutational analysis of a catalytically important loop containing active site and substrate-binding site in Escherichia coli phytase AppA. *Biosci. Biotechnol. Biochem.* **2019**, *83*, 860–868. [CrossRef] [PubMed]
23. Li, X.; Chen, B.; Chen, W.; Pu, Z.; Qi, X.; Yang, L.; Wu, J.; Yu, H. Customized multiple sequence alignment as an effective strategy to improve performance of Taq DNA polymerase. *Appl. Microbiol. Biotechnol.* **2023**, *107*, 6507–6525. [CrossRef] [PubMed]
24. Chovancova, E.; Pavelka, A.; Benes, P.; Strnad, O.; Brezovsky, J.; Kozlikova, B.; Gora, A.; Sustr, V.; Klvana, M.; Medek, P.; et al. CAVER 3.0: A tool for the analysis of transport pathways in dynamic protein structures. *PLoS Comput. Biol.* **2012**, *8*, e1002708. [CrossRef] [PubMed]
25. Jumper, J.; Evans, R.; Pritzel, A.; Green, T.; Figurnov, M.; Ronneberger, O.; Tunyasuvunakool, K.; Bates, R.; Zidek, A.; Potapenko, A.; et al. Highly accurate protein structure prediction with AlphaFold. *Nature* **2021**, *596*, 583–589. [CrossRef] [PubMed]
26. Morris, A.L.; MacArthur, M.W.; Hutchinson, E.G.; Thornton, J.M. Stereochemical quality of protein structure coordinates. *Proteins* **1992**, *12*, 345–364. [CrossRef] [PubMed]
27. Laskowski, R.A.; Rullmannn, J.A.; MacArthur, M.W.; Kaptein, R.; Thornton, J.M. AQUA and PROCHECK-NMR: Programs for checking the quality of protein structures solved by NMR. *J. Biomol. NMR* **1996**, *8*, 477–486. [CrossRef] [PubMed]
28. Sippl, M.J. Recognition of errors in three-dimensional structures of proteins. *Proteins* **1993**, *17*, 355–362. [CrossRef]
29. Wiederstein, M.; Sippl, M.J. ProSA-web: Interactive web service for the recognition of errors in three-dimensional structures of proteins. *Nucleic Acids Res.* **2007**, *35*, W407–W410. [CrossRef]
30. Trott, O.; Olson, A.J. AutoDock Vina: Improving the speed and accuracy of docking with a new scoring function, efficient optimization, and multithreading. *J. Comput. Chem.* **2010**, *31*, 455–461. [CrossRef]
31. Notredame, C.; Higgins, D.G.; Heringa, J. T-Coffee: A novel method for fast and accurate multiple sequence alignment. *J. Mol. Biol.* **2000**, *302*, 205–217. [CrossRef]
32. Crooks, G.E.; Hon, G.; Chandonia, J.M.; Brenner, S.E. WebLogo: A sequence logo generator. *Genome Res.* **2004**, *14*, 1188–1190. [CrossRef]

Disclaimer/Publisher's Note: The statements, opinions and data contained in all publications are solely those of the individual author(s) and contributor(s) and not of MDPI and/or the editor(s). MDPI and/or the editor(s) disclaim responsibility for any injury to people or property resulting from any ideas, methods, instructions or products referred to in the content.